Spatial–Temporal Variations and Mechanisms of the Upper Ocean Heat Content in the South China Sea

Hongwei Liu,[1,4] Qilong Zhang,[1,4] Chongguang Pang,[1,4] Rongshuo Cai,[2] Qinghua Qi,[2] and Dongmei Zheng[3]

Abstract—The variability of the upper ocean heat content (OHC) of the South China Sea (SCS) has a significant regional climate impact on the surrounding East and Southeast Asian countries. In this paper, the spatial–temporal variations of the upper OHC in the SCS and their relations to El Niño-Southern Oscillation (ENSO) are analyzed using empirical orthogonal functions and correlation analysis. The mechanisms for the interannual OHC variability associated with ENSO and regime shift in 1998 are further examined using composite and correlation analysis methods. The results show that the OHC anomaly field is mainly composed of two leading modes, i.e., an in-phase oscillation mode and a zonal anti-phase oscillation mode. The in-phase oscillation mode exhibits strong interannual variability with periods of 2–5 years, which is well related to ENSO at a lead of 6 months, and experienced a regime shift in 1998. The anti-phase oscillation mode shows only a strong interannual variability with periods of 2–4 years well related to ENSO at a lag of 4 months. The composite analysis reveals that horizontal thermal advection mainly controlled by wind forcing plays a primary role in modulating the interannual OHC variability associated with ENSO, while net surface heat flux is the secondary source. And the OHC regime shift in 1998 primarily results from both the strong cold advection during the extremely strong El Niño in 1997 and the subsequent warm advection during the strong La Niña in 1998.

Key words: The South China Sea, Heat content, spatial and temporal variation, regime shift.

[1] Key Laboratory of Ocean Circulation and Waves, Institute of Oceanology, Chinese Academy of Sciences and Qingdao National Laboratory for Marine Science and Technology, 7 Nanhai Road, Qingdao 266071, People's Republic of China. E-mail: liuhongwei@qdio.ac.cn

[2] Key Laboratory of Global Change and Marine-Atmospheric Chemistry, Third Institute of Oceanography, State Oceanic Administration, Xiamen 361005, China.

[3] Marine Environmental Forecasting and Disaster Preventing and Reeducing Center of Liaoning Province, Shenyang 110001, China.

[4] Center for Ocean Mega-Science, Chinese Academy of Sciences, 7 Nanhai Road, Qingdao 266071, People's Republic of China.
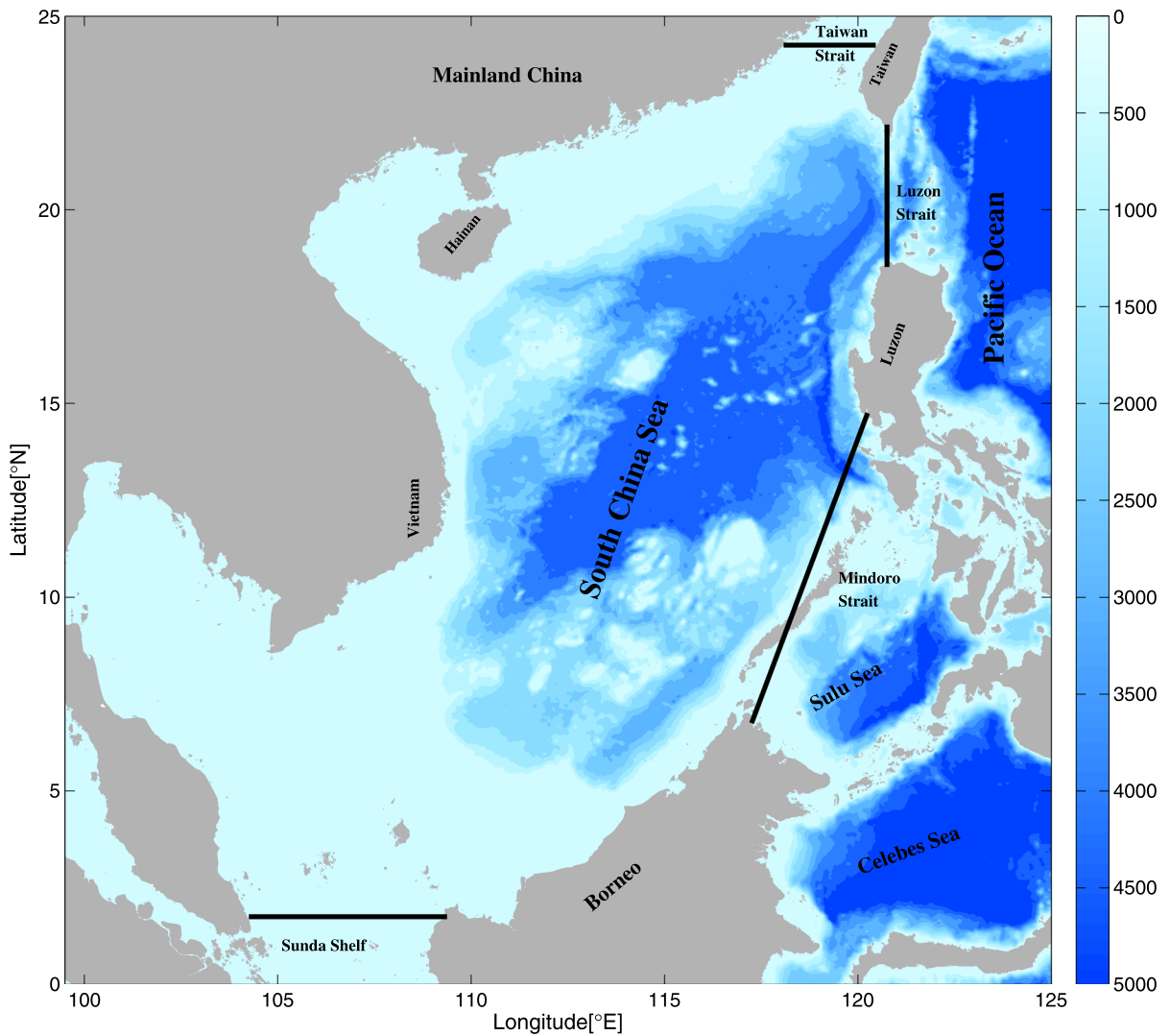
1. Introduction

The South China Sea (SCS) is the largest marginal sea in the western North Pacific, with a total area of 3.5 million km^2 and an average depth of over 2000 m. It is a semi-enclosed basin that connects to and exchanges water with the Southeast Asian waters (Fig. 1). In addition, as an important part of the tropical Pacific-Indian Ocean warm pool and a sensitive area of atmosphere–ocean interaction, the SCS not only plays an import role in the onset of the SCS summer monsoon (Zhao and Chen 2000; Xie et al. 2003; Wang et al. 2004; Lai et al. 2011; Qi and Cai 2014), but also has an significant effect on the summer precipitation in the mid-lower valleys of the Yangtze River and in southern China (Jin and Luo 1986; Zhang et al. 2003; Zhou et al. 2010). Therefore, the role of the SCS in climate change is being paid more attention by scientists, and extensive researches on the SCS have been conducted.

Because the sea surface temperature (SST) and the heat content are two important parameters that characterize the thermal state of the SCS, scientists have carried out extensive research on the spatial–temporal variations of the SCS SST since the 1990s (Niu 1994; Chu et al. 1997; Chu and Chang 1997; Ose et al. 1997; Klein et al. 1999; Wang et al. 2002, 2006; Cai et al. 2009). The previous studies showed that the interannual variability in the SCS SST is well associated with El Niño-Southern Oscillation (ENSO) and the SSTs are higher (lower) than normal during El Niño (La Niña) events, while the influence of ENSO on the SCS SST is mainly achieved through the atmospheric bridge (Klein et al. 1999; Wang et al. 2000). However, there have been relatively few studies on the OHC in the SCS, and the

Figure 1
Bottom topography of the SCS based on the 2-min gridded global relief data (ETOPO2) from https://www.ngdc.noaa.gov/mgg/global/relief/ETOPO2/ETOPO2v2-2006. The four black lines are used for illustrating the heat transports in Sect. 4

results obtained from different datasets are also quite different from each other (Chen et al. 2013). Using vertically averaged temperatures from the surface to the 100-m depth from 1959 to 1998 and Southern Oscillation index, He and Guan (1997) reported that the OHC in the SCS has significant interannual variability with periods of 2 and 4–5 years, and is well related to ENSO at a lag of 6 months, which is consistent with the results obtained by Cai et al. (2009) using SST data and Niño3 index. From the OHC anomaly in the SCS estimated by using merged

altimetry data from 1992 to 2004, Tong et al. (2006) found that the OHC anomaly has approximately 0.5, 1.5, 2.4, 4 and 6 years oscillations besides the annual cycle and underwent an abrupt change in 1998. Recently, Yan et al. (2010) analyzed the interannual variability in the OHC of the SCS and its response to ENSO using vertically averaged temperature from the surface to the 300-m depth during 1987–2006 from the Japan Meteorological Agency and Niño3 index, and pointed out that the first mode of the OHC anomaly field is an east–west tilting mode with

periods of 2–7 years and is well related to ENSO without time lag, which is quite different from He and Guan's results (1997). In addition, using SODA temperature data from the surface to the 400-m depth, Song et al. (2014) found that the OHC in the SCS displays a significant decadal variability and decreased (increased) during 1958–1968 and 1982–1992 (during 1969–1981 and 1993–2003).

It should be also noted that previous studies used only the sum of upper sea temperatures as the OHC, and did not consider the contribution of salinity to the OHC. Strictly speaking, the sum of sea temperatures is not the real OHC. Moreover, the calculation depth also has an important effect on the estimation of OHC. If the selected depth is too shallow (≤ 100 m), the resulting OHC is unable to reflect the thermodynamic characteristics and dynamic process in the upper ocean such as SST, since the OHC variations in thermocline are larger than that in the upper mixed layer (Wu et al. 2011). Besides, there are still different views on the mechanism responsible for OHC interannual variability. For example, Qu et al. (2004) emphasized the role of oceanic bridge and pointed out that the water transport of Luzon Strait between the SCS and the Pacific Ocean is a key process conveying the ENSO signal into the SCS and influencing its circulation and OHC using the results from a high-resolution ocean general circulation model, while Yan et al. (2010) suggested that wind stress curl and latent heat flux are the main driving elements for the interannual variability in the OHC. In addition, Song et al. (2014) argued that the advection and the net surface heat flux have significant influences on the decadal variability of the OHC in the SCS. However, the mechanism for the regime shift of the OHC in 1998 is not yet clear. The intent of this study is to discuss these questions by using the monthly mean temperature and salinity data, SODA data and NCEP reanalysis data. After a brief description of both the data and methodology in Sect. 2, the spatial and temporal variations of the OHC in the SCS are analyzed in Sect. 3. Section 4 examines the mechanisms for the interannual variability and regime shift in the OHC, and results are summarized in Sect. 5.

2. Data and Methodology

2.1. Data Description

In the present study, the monthly averaged sea temperature and salinity data are used to calculate the OHC in the SCS. This dataset is an objective analysis data provided by the Japan Meteorological Agency (Ishii et al. 2003, 2006). The data set covers the global ocean with a horizontal resolution of 1°latitude × 1°longitude and 24 standard vertical layers during the period 1945–2012 and in the upper ocean. Only the temperature and salinity data in the SCS (0°–25°N, 99°–125°E) during the period of 1950–2012 are used in this paper.

The monthly sea current and temperature data in the upper ocean are extracted from the Texas A&M University, Carton-Giese SODA version 2.2.4 version during period 1871–2010 with a resolution of 0.5° × 0.5° (Carton and Giese 2008; Giese and Ray 2011). This data set combined a wide variety of observations and numerically simulated results. We use only the flow velocity and temperature data in the SCS during 1950–2010 in this paper. The validation by comparing with the observations (Chen et al. 2013) increases our confidence in the validity of the dataset.

The monthly wind and sea surface heat flux data are obtained from the NCEP (National Centers for Environmental Prediction, USA) reanalysis data set (Kalnay et al. 1996). The data set covers almost the whole globe with Gaussian grid from 1948 to the present. The wind and net sea surface heat flux data in the SCS during the period 1950–2012 are used in this paper.

The time series of the monthly Niño 4 index, the regional averaged SST anomalies in the Niño 4 area (5°S–5°N, 160°E–150°W), are derived from the National Centers for Environmental Prediction/Climate Prediction Center (NCEP/CPC) to indicate the Central-Pacific (CP) ENSO event during 1950–2012.

2.2. Methodology

We calculate the OHC from the surface to a 400 m depth at each grid point in the SCS (0°–25°N, 99°–125°E) according to the following formula,

$$Q = \int C_p \rho T \mathrm{d}z, \qquad (1)$$

where, C_P is the specific heat capacity at constant pressure for seawater, ρ is sea water density, and T is sea water temperature. Both ρ and C_P are calculated from the temperature, salinity and depth in the text and all the data set is from the Japan Meteorological Agency.

Since the variation of the OHC is mainly caused by the variation of heat content in both the mixed layer and the thermocline over the western Pacific Ocean (Wu et al. 2011), the optimum depth for calculating the OHC should be determined by the lower boundary depth of the thermocline. In the SCS, the strongest thermocline is 200 m thick, and its lower boundary is located at a depth of 400 m (Zhou 2002), so it is appropriate to use 400 m as the depth to calculate the OHC in the SCS, which is also consistent with the depth in Qu et al. (2004).

The water exchange between the SCS and its surrounding waters is carried out mainly through the Luzon Strait, the Taiwan Strait, the Mindoro Strait and the Sunda Shelf. In order to discuss the influence of the horizontal thermal advection on the OHC, therefore, we calculated the heat transports through these straits and the Sunda Shelf, respectively, using the following formula in Sect. 4.

$$Q = \iint C_P \bullet \rho \bullet (\theta - \theta_0) \bullet V \mathrm{d}x \mathrm{d}z, \qquad (2)$$

where, C_P and ρ are the same as those in Formula (1), θ is potential temperature, θ_0 is an arbitrary temperature reference and V is the flow velocity normal to the section. A meaningful estimate of the meridional ocean heat flux requires the calculation of over a full oceanic section for which there is zero net mass transport; otherwise the calculated heat transport is dependent on an arbitrary temperature reference (Fillenbaum et al. 1997; Johns et al. 2011). The depth of θ_0 and the accumulated depth is taken as 400 m (the sea bottom) in the waters deeper (shallower) than 400 m. Using the velocity, sea temperature and salinity data in the SODA dataset in the period of 1950–2010, we calculate the heat transports through the Luzon Strait (120.75°E, 18.25°–22.25°N), the southern Taiwan Strait (24.25°N, 117.25°–120.25°E),

the Mindoro Strait (We choose an oblique section in the box of 117.25°–120.25°E and 6.75°–14.75°N), and the Sunda Shelf (1.75°N, 104.25°–111.25°E), respectively, (the black lines in Fig. 1). In order to be consistent with the OHC, the heat transport anomalies are obtained by removing the monthly mean values and filtering their annual cycle signal using a 13-month running mean.

The method of Empirical orthogonal functions (EOF) is used to analyze the spatial and temporal variability of the SCS heat content anomaly field. The anomaly field is obtained by removing the monthly mean values and then filtering their annual cycle signal using a 13-month running mean. Moreover, the power spectrum and composite analysis methods are also used to examine the dominant periods and mechanisms for spatial and temporal variability of the anomaly field.

3. Temporal and Spatial Variations of the OHC

Figure 2 shows the mean field climatological distribution of the OHC in the SCS. In general, the OHC is low ($< 15.0 \times 10^9$ Jm^{-2}) in the shallow waters and high ($> 25.0 \times 10^9$ Jm^{-2}) in the deep waters with a maximum of 30.85×10^9 Jm^{-2} in the central Luzon Strait. Then, what is the spatial and temporal variability in the OHC? For this, we analyzed the spatial and temporal characteristics of the OHC anomaly field using the EOF method in this section. The EOF analysis results show that the variance contributions of the first two modes are much larger than that of the others, which can explain 66.8% of their total variance. Therefore, these two dominant modes are discussed only in this section.

3.1. The First Mode of the OHC Anomaly Field

The first mode (EOF1) of the OHC anomaly field can explain 48.4% of the total variance. Its spatial pattern (Fig. 3a) displays consistent oscillation characteristics in the whole basin (being called an in-phase oscillation mode), and the high value area ($> 0.075 \times 10^9$ Jm^{-2}) is located in the central SCS (12.5°–17.5°N, 114°–118°E), slightly eastward from the results obtained using the OHC anomaly field
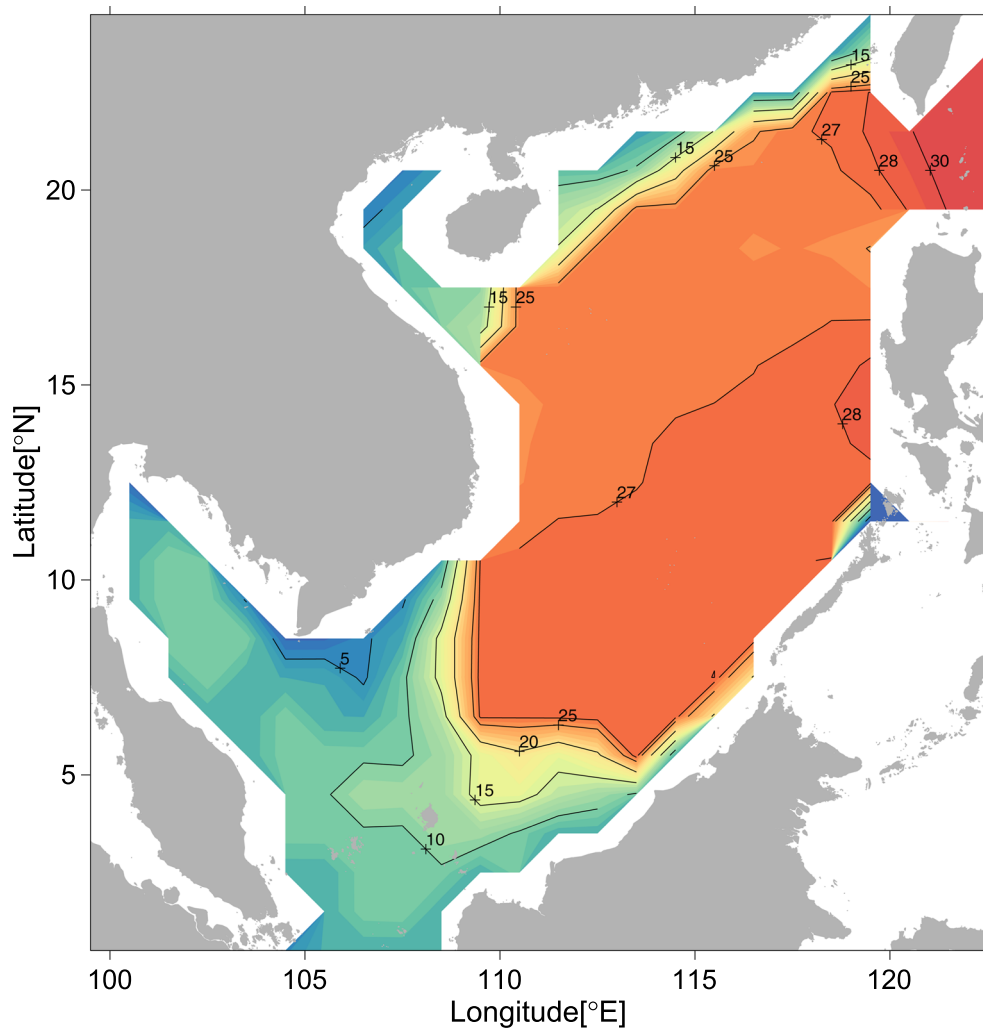
Figure 2
The mean field climatological distribution of the OHC in the South China Sea

from the surface to 100 m depth (He and Guan 1997) and the SST anomaly field (Cai et al. 2009). The principal component of the EOF1 mode (PC1) displays significant interannual variability with periods of 2–5 years (Fig. 3c), and it is related to the Niño 4 index at a lead of 6 months ($r = -0.44$), showing that the OHC might have dropped (risen) to the lowest (highest) values when El Niño (La Niña) event reached its mature phase 6 months before (Fig. 3d). This is different from the results obtained by Yan et al. (2010), who examined 2–7 years period variations of the OHC and its relation to ENSO based on the sea temperatures from the sea surface to the

depth of 300 m and Niño 3 index. Moreover, this 6 months lead between the PC1 and Niño 4 index has never been reported in previous studies (He and Guan 1997; Yan et al. 2010).

It is worth noting that during 1950–2012, there are eleven CP-El Niño events (1957/1958, 1963/1964,1965/1966,1968/1969,1977/1978,1986/ 1988,1991/1992,1994/1995,2002/2003,2004/2005 and 2009/2010) and seven CP-La Niña events (1973/ 1974,1974/1976,1984/1986,1988/1989, 1998/2000, 2007/2008 and 2011/2012). In order to verify the relationship between the PC1 and the CP-ENSO, the composite analysis is carried out using these CP-El
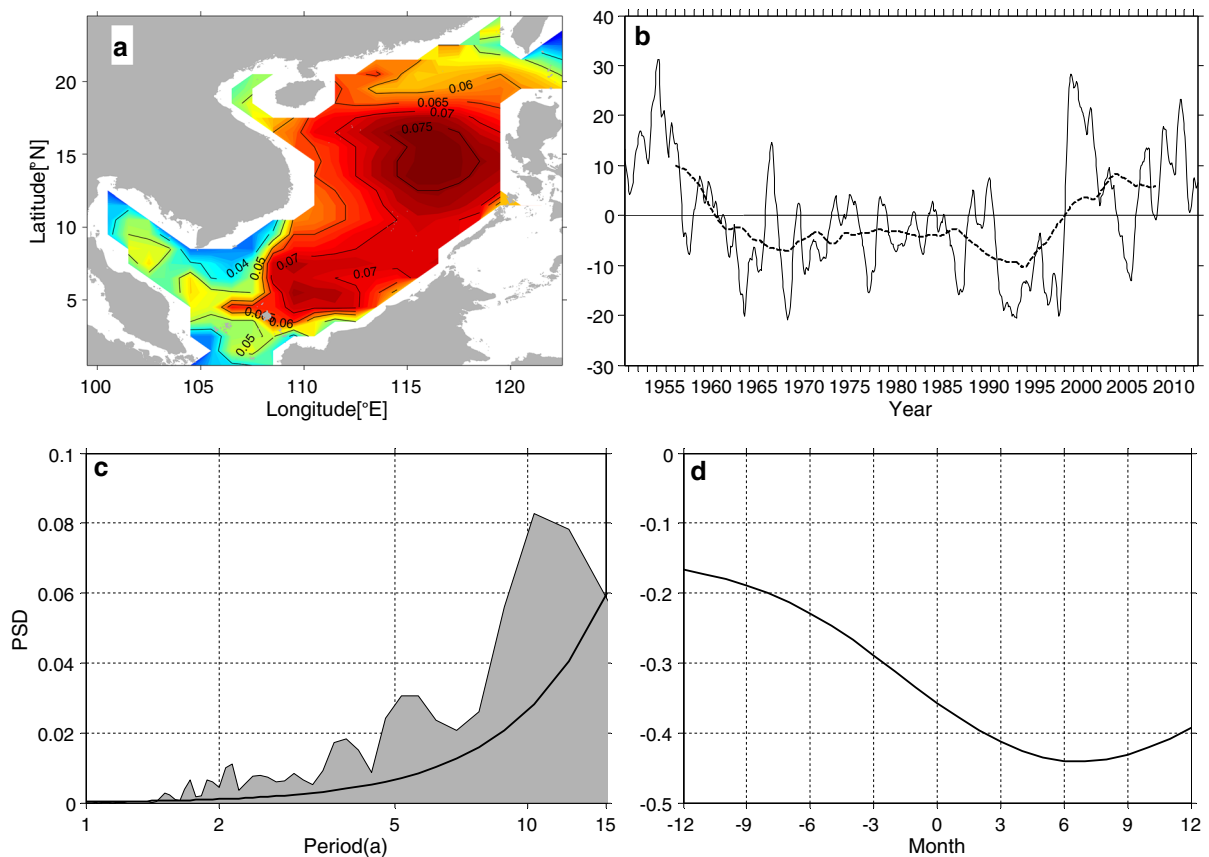
Figure 3
a Spatial pattern and **b** principal component of the first EOF mode in the OHC anomaly field (The dotted line is the 120-month running mean result), **c** power spectra of the principal component with the 95% confidence level (black line), and **d** the lagged correlation between PC1 and Niño 4 index

Niño and CP-La Niña events. In the following analysis, [0] and [+ 1] denote the El Niño or La Niña year and the subsequent year, respectively. Note that the mature phases of the composited El Niño and La Niña events appear in December [0] and March [+ 1], respectively (not shown). Figure 4a displays the mean PC1s for the 11 El Niño (solid line) and 7 La Niña events (dotted line) during year [0] and [+ 1], respectively. It can be found from Fig. 4a that the PC1 is negative during the El Niño year with a minimum of − 9.34 in June [0], but it becomes positive during the La Niña year with a maximum of 7.09 in September [0], which is consistent with the correlation analysis results above. This implies that the OHC is low during El Niño event and high during

La Niña event, which is contrary to the SCS SST (Cai et al. 2009).

In addition, this mode also shows an interdecadal variability (the dotted line in Fig. 3b) with a period of 10 years (Fig. 3c). From the beginning of the 1960s to the end of the 1990s, the PC1 is negative, i.e., the OHC is in the low stage, while before 1960s and after the end of 1990s, the PC1 is positive, i.e., the OHC is in the high stage, which is consistent with results obtained by Song et al. (2014) using the SODA product. The analysis of a *t* test with a 10-year running mean filter indicates that the PC1 experienced a regime shift in 1998, which also agrees with results of Tong et al. (2006)' results. The mean PC1 is − 5.67 during 1961–1998 and 8.42 during 1999–2012 with a difference of 14.09.
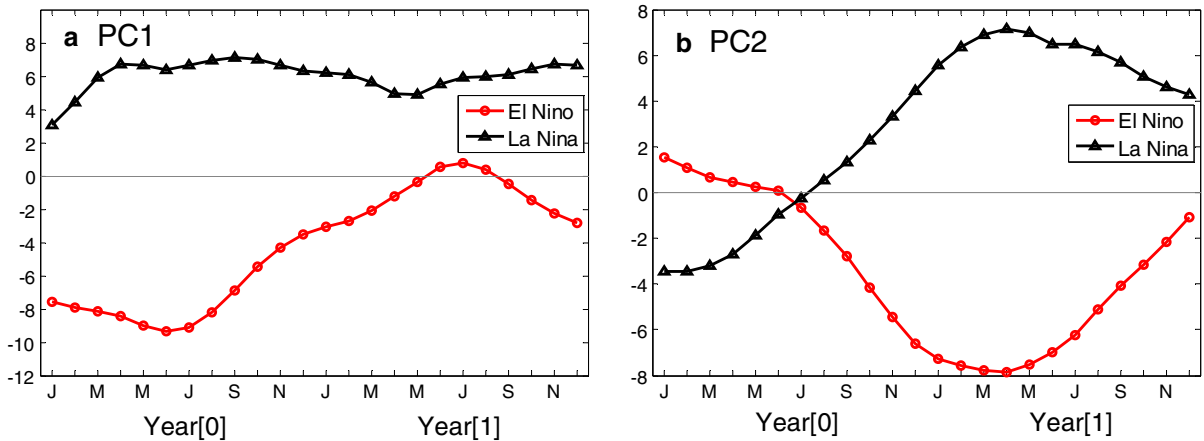
Figure 4
The mean **a** PC1 and **b** PC2 for 11 El Niño and 7 La Niña events

3.2. The Second Mode of the OHC Anomaly Field

The second mode (EOF2) of the OHC anomaly field in the SCS can explain 18.4% of the total variance, and it displays a zonal anti-phase oscillation in the whole basin, especially in the southern part of the SCS (Fig. 5a). When the principal component of EOF2 mode (PC2) is positive, the local maximum positive values ($\geq 0.05 \times 10^9 \ \mathrm{Jm}^{-2}$) are centered in the southeast SCS and the northwest off Luzon Island, which are closely related to the most sensitive area to water exchange between the SCS and the western Pacific or the Sulu Sea (Qu et al. 2004), while the local maximum negative values ($\leq -0.09 \times 10^9 \ \mathrm{Jm}^{-2}$) are found in the Sunda Shelf and adjacent waters. The PC2 still has significant interannual variability (Fig. 5b) and is closely related to the ENSO cycle, but smaller than the PC1 (Fig. 3b) in amplitude. The PC2 is negative during most El Niño events, and it becomes positive during most La Niña events. A power spectrum analysis shows that the main periods of PC2 are 3.7, 2.5 and 6.9 years, respectively (Fig. 5c), indicating that the second mode contains strong interannual variability with periods of 2–7 years and very weak interdecadal variability. A cross-correlation analysis also shows that the PC2 is closely related to the Niño 4 index at a lag of 4 months ($r = -0.70$) (Fig. 5d), which is also confirmed by the composite analysis (Fig. 4b). In Fig. 4b the PC2 is negative during the El Niño event

after July [0] with a minimum of -7.86 in April [$+1$], and it is positive during the La Niña event after August [0] with a maximum of 7.15 in April [$+1$]. This implies that when the El Niño(La Niña) event reaches its mature phase 4 months (1 month) later, the OHC in the eastern SCS would reduce to a minimum (rise to a maximum), while the OHC in the western SCS would be in contrary condition, which is also different from the results (an in-phase oscillation mode) obtained by Yan et al. (2010).

In summary, the OHC anomaly field in the SCS is mainly composed of both an in-phase oscillation mode and a zonal anti-phase oscillation mode. The in-phase oscillation mode has a strong interannual variation with periods of 2–5 years and is well related to the ENSO at a lead of 6 months besides a regime shift in 1998. The anti-phase oscillation mode has significant interannual variation with periods of 2–7 years and is closely related to ENSO at a lag of 4 months.

4. Mechanisms for the OHC Interannual Variability and Regime Shift

The first mode of the OHC anomaly field is well related to the ENSO at a lead of 6 months and experienced a regime shift in 1998. As mentioned above, the influence of ENSO can be transferred into the SCS through the atmospheric and ocean bridges,
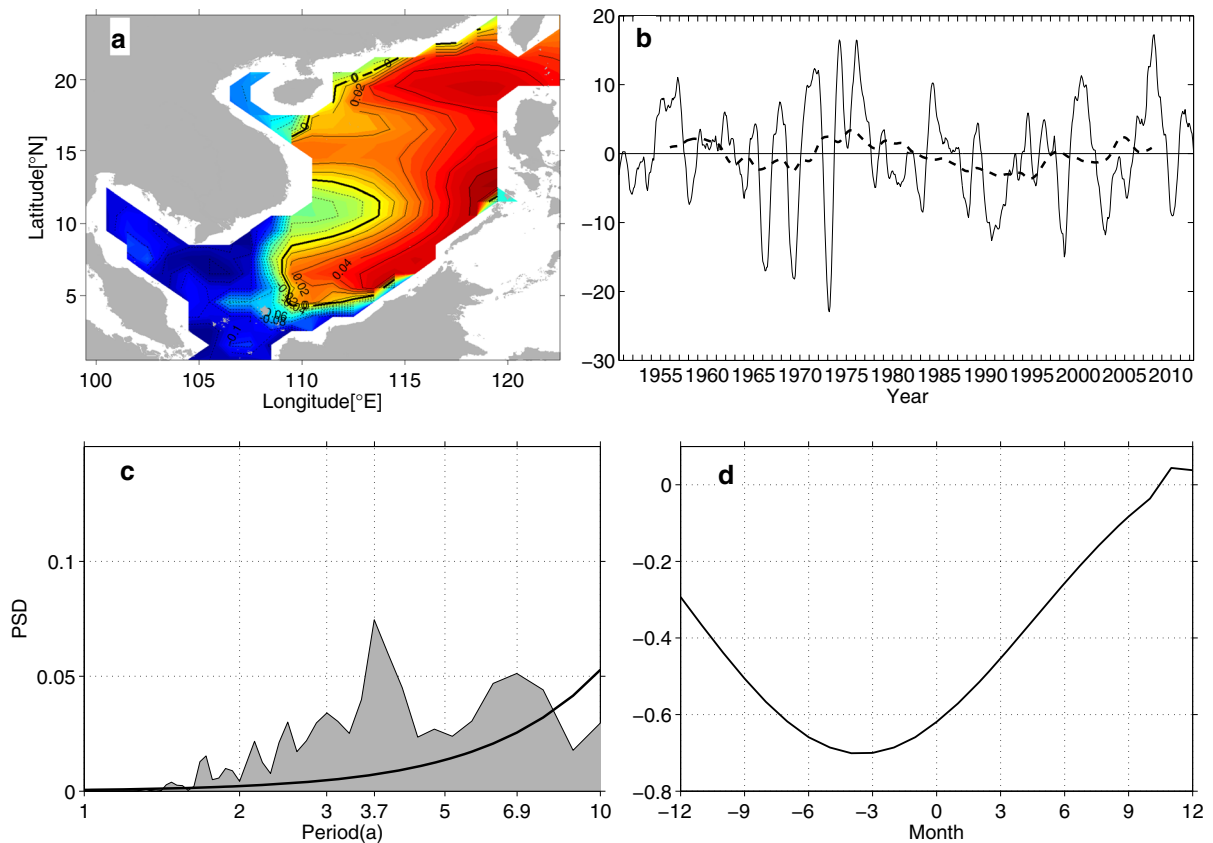
Figure 5
a Spatial pattern and **b** principal component of the second EOF mode in the OHC anomaly field (The dotted line is the 120-month running mean result), **c** power spectra of the principal component with the 95% confidence level (black line), and **d** the lagged correlation between PC2 and Niño 4 index

which can induce changes of surface wind, surface heat fluxes and ocean circulations. So far, however, the mechanism for the regime shift in 1998 is not yet clear. In this section, therefore, we examine the roles played by the surface wind stress, surface heat flux, and ocean thermal advection, respectively.

A cross-correlation analysis shows that the correlation between the PC1 and the OHC anomaly in the whole basin is 0.81 at zero lag, which can explain the 65% of the OHC variation. In the following analysis, therefore, the OHC anomaly is used to examine the mechanisms for its interannual variability and regime shift in 1998.

4.1. Mechanism for the Interannual Variability

In order to examine the influence of wind stress, heat transports and net heat flux on the OHC in the SCS during ENSO, we performed the composite analyses of these variables in eleven El Niño and seven La Niña events, respectively, and the results are shown in Figs. 6, 7, 8. Owing to space limitations, however, Fig. 6 (Fig. 7) show only the wind tress anomaly field in February, May, August and November of the El Niño (La Niña) year.

Previous studies reported that the SCS generally experiences winter and summer monsoons every year (Peter et al. 1997). During the winter monsoon season, a cold northeasterly wind blows over the SCS. Such a typical winter monsoon pattern lasts 6 months (from November to April). During the
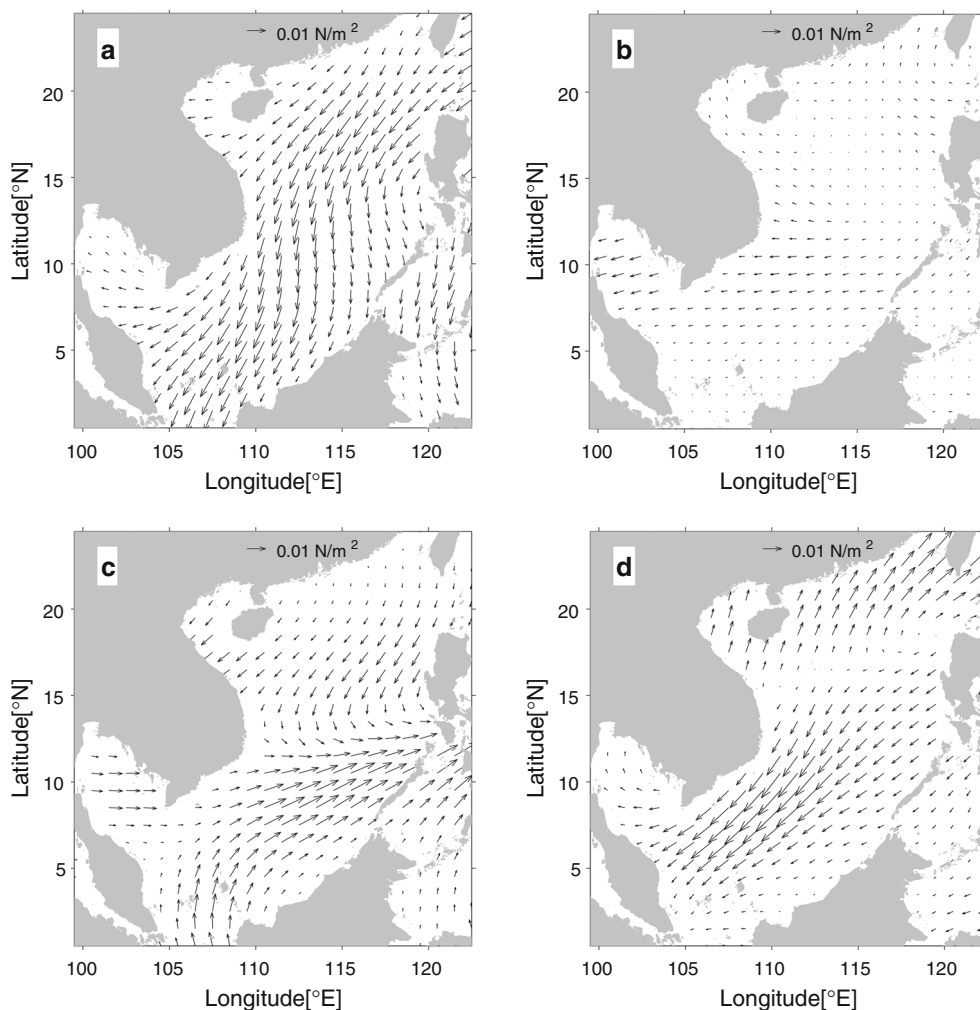
Figure 6
Composite wind stress anomaly over the SCS in four seasons of the El Niño year. **a** In winter (February), **b** in spring (May), **c** in summer (August), and **d** in autumn (November)

summer monsoon season, a warm and weaker southwesterly wind blows over the SCS. Such a typical summer monsoon pattern lasts 4 months (from May to September). Then, how does the wind stress over the SCS during the El Niño (La Niña) year? Thus, this issue will be discussed in the following analysis.

4.1.1 During El Niño Year

During winter season of El Niño year (January–April), the SCS is primarily controlled by the anomalous northeasterly wind (Fig. 6a), similar to a

normal winter monsoon pattern. Such a wind field favors the enhancement of cold advection. As shown in Fig. 8a–d (red line), the heat transport in the Luzon Strait, called the Luzon Strait heat transport (LSHT) hereinafter, has larger negative anomalies during January–April, the heat transport in the Taiwan Strait, called the Taiwan Strait heat transport (TSHT) hereinafter, is changed from a positive anomaly during January–February to a negative anomaly during March–April, the heat transport in the Mindoro Strait, called the Mindoro Strait heat transport (MSHT) hereinafter, is a negative anomaly during January–April, while the heat transport in the Sunda
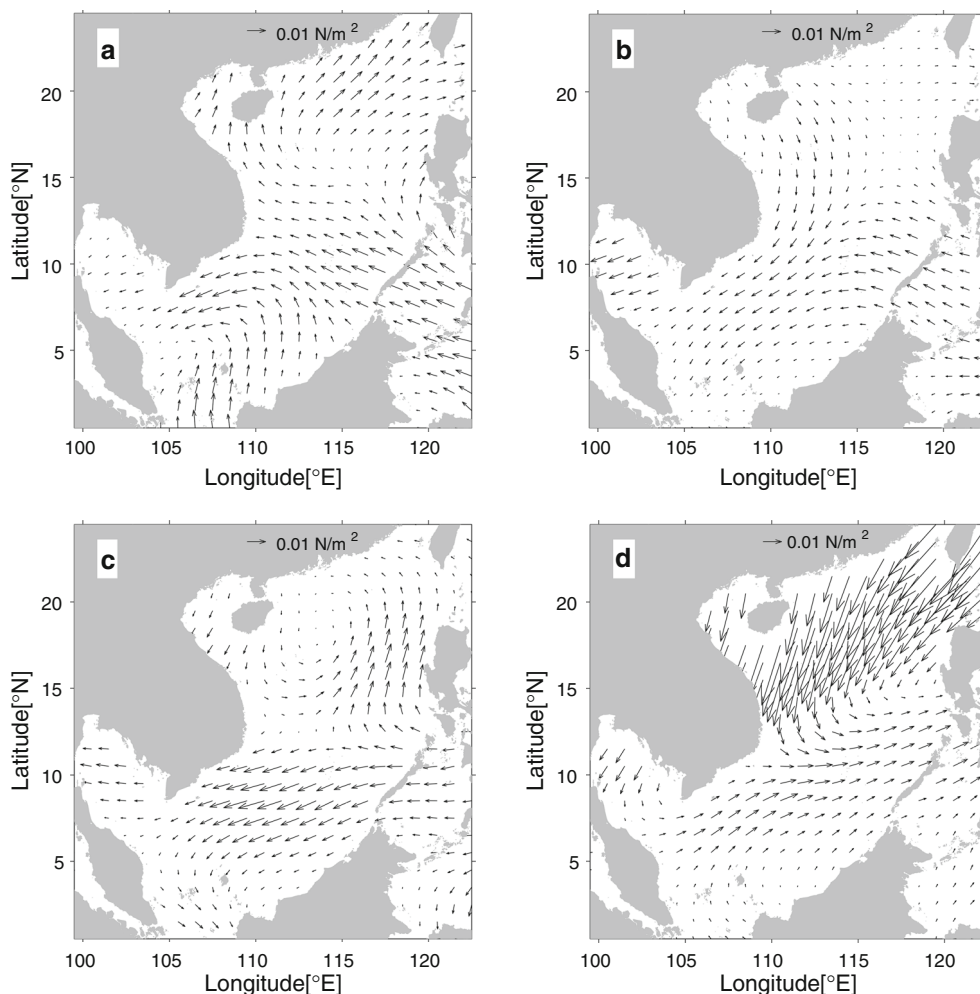
Figure 7
The same as Fig. 6 but in the La Niña year

Shelf, called the Sunda Shelf heat transport (SSHT) hereinafter, is the smallest positive anomaly during January–April than for the other three straits. Usually, the sum of these heat transports is called the SCS through flow heat transport (SCSTHT), and when the SCSTHT is a positive (negative) anomaly, there is a warm (cold) advection in the SCS. During January–April, the SCSTHT is a negative anomaly (Fig. 8e, red line), and a cold advection exists in the SCS. Meanwhile, the SCS has been releasing heat into the overlying atmosphere with a maximum anomaly of -1.27×10^{10} W in March (Fig. 8f). As a result, the OHC is continuously reduced with a minimum anomaly of -9.06×10^{22} J in April.

The wind fields during summer season (May to September) of an El Niño year are very different from those during the winter season. In May, the weaker anomalous southerly and easterly winds occur over the Taiwan Strait and the Luzon Strait, respectively, while the stronger anomalous easterly winds are found over the central-southern SCS (6°–13°N) (Fig. 6b). After that, the anomalous southwesterly wind prevails over the southern SCS, while the wind field over the northern SCS is changed from month to month. For example, the northern SCS is primarily controlled by the anomalous southwesterly in June, but by the anomalous southeasterly wind in July (not shown). The anomalous northeasterly prevails over
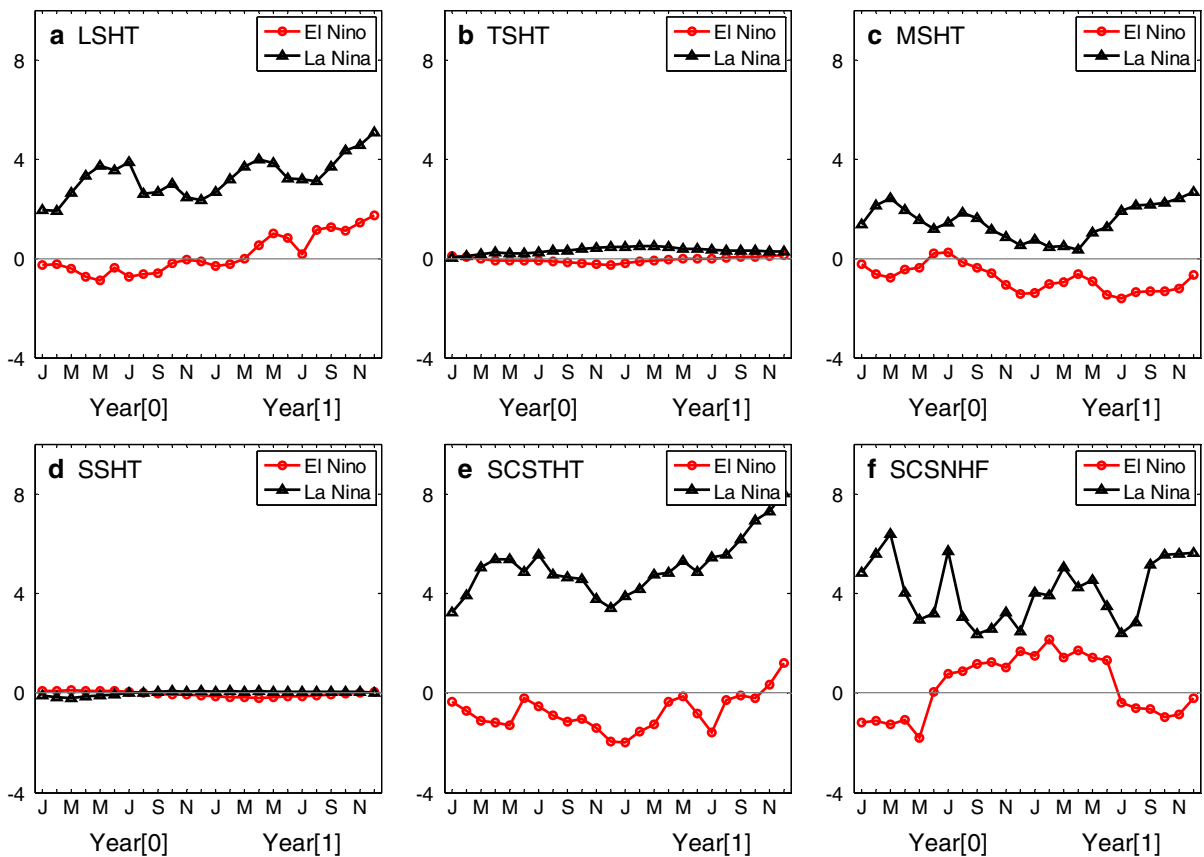
Figure 8
Annual cycles of the composite heat transport anomaly through **a** the Luzon Strait, **b** the Taiwan Strait, **c** the Mindoro Strait and **d** the Sunda Shelf, **e** the composite the SCSTHT anomaly (Unit: 10^{13} W) and **f** the net surface heat flux anomaly in the SCS (Unit: 10^{10} W) during El Niño and La Niña event

the northern SCS in August (Fig. 6c), while the weaker anomalous westerly blows over the Luzon Strait in September (not shown). These wind fields can help the surrounding seawater enter the SCS. As shown in Fig. 8a–d (red line), during May–September, the LSHT and TSHT are a negative anomaly, the MSHT is a negative anomaly, except for a small positive anomaly during June–July, while the SSHT is a small positive anomaly except for a small negative anomaly in September. Thus, the cold advection is stronger during this period, and the SCSTHT is a negative anomaly with a minimum of -1.30×10^{13} W in May (Fig. 8e, red line). On the other hand, the SCS gets heat during June–September except to release heat in May (Fig. 8e, red line). As a result, having reached its lowest value with an

anomaly of -10.18×10^{22} J in June, and then the OHC begins to increase slowly, but is still lower with an anomaly of -8.27×10^{22} J in September. Note that the lowest PC1 (OHC) in June may be primarily induced by the cold LSHT with a minimum anomaly of -0.90×10^{13} W and the heat release of the SCS with a minimum anomaly of -1.81×10^{10} W in May.

When El Niño is going to reach its mature period (October–December), the wind field over the SCS has changed significantly. Except for the anomalous southwesterly wind north of 19°N, most of the SCS are still controlled by the anomalous northeasterly wind during October–November (Fig. 6d). In December, however, the anomalous southwesterly wind over the northern SCS (north of 12°N) strengthens greatly,

while anomalous southeasterly wind blows over the Sunda Shelf (not shown). These wind fields are basically favorable to the outflow of the SCS water. During October–December, as shown in Fig. 8a–d (red line), the LSHT is a positive anomaly, while the TSHT, MSHT and SSHT are all a negative anomaly. Thus, there is a stronger cold advection in the SCS, and the SCSTHT is negative anomaly during this period (Fig. 8e, red line). Meanwhile, the SCS also gets heat from the overlying atmosphere, and the net surface heat flux anomaly reaches a maximum $(1.67 \times 10^{10}$ W) in December (Fig. 8f, red line). Thus, the OHC is increasing slowly, but it is still lower, whose anomaly is negative with an anomaly of -5.66×10^{22} J in December.

4.1.2 During a La Niña Year

During the winter season of a La Niña year, the wind stress anomaly field over the SCS is basically contrary to the winter monsoon pattern of an El Niño year. During January–April, the strong anomalous southerly to southeasterly winds prevail over the southern SCS (south of 15°N), while anomalous southwesterly wind blows over the northern SCS. Figure 7a shows a typical winter monsoon pattern in February. These wind fields not only drive the warm water outside into the SCS through the Sunda Shelf and the Mindoro Strait, but also force the cold SCS water to flow out of the SCS through the Luzon Strait and the Taiwan Strait. As shown in Fig. 8a–d (black line), the LSHT, TSHT and MSHT are a positive anomaly during January–April, while the SSHT is a small negative anomaly during January–April. Thus, the warm advection strengthens slowly, and the SCSTHT is a positive anomaly with a range of $3.25–5.38 \times 10^{13}$ W during January–April (Fig. 8e, black line). Meanwhile, the SCS gets heat from the overlying atmosphere, and the net surface heat flux is a positive anomaly (Fig. 8f, black line). Both the enhancement of warm advection and the increase of obtained heat lead the OHC to increase significantly, whose anomaly is increased from 6.87×10^{22} J in January to 12.24×10^{22} J in April.

The wind fields during a summer season (May to September) of a La Niña year are very different from the winter monsoon pattern. Excepting the strong

anomalous easterly to southeasterly wind over the Sulu Sea, the southern SCS is primarily controlled by the anomalous northeasterly wind, which is strongest in July and weakest in May, while the wind stress over the northern SCS is changed. During May–July, the weaker anomalous westerly-northwesterly wind blows over the Luzon Strait and the Taiwan Strait (Fig. 7b). In August, however, owing to an anomalous cyclone circulation over the northern SCS, the weaker southerly wind blows over the Luzon Strait, while the weaker easterly wind does so over the Taiwan Strait (Fig. 7c). In September, the weaker southwesterly wind prevails over the Luzon Strait and the Taiwan Strait (not shown). The strong northeasterly wind over the southern SCS helps the water there flow out of the SCS through the Sunda Shelf, the weaker westerly-northwesterly or weaker southwesterly wind over the northern SCS favors the water there to flow out of the SCS through the Luzon Strait and the Taiwan Strait, but the strong southeasterly wind drives the warm water in the Sulu Sea into the SCS through the Mindoro Strait. Thus, the SSHT is a negative anomaly during May–June, but becomes a positive anomaly during July–September, while the LSHT, TSHT and MSHT are all a positive anomaly during May–September (Fig. 8a–d, black line). The warm advection is stronger during this period, and the SCSTHT is a positive anomaly with a maximum of 5.55×10^{13} W in July (Fig. 8e, black line). Meanwhile, the SCS still gets heat from the overlying atmosphere with a net surface heat flux anomaly range of $2.35–5.71 \times 10^{10}$ W (Fig. 8f, black line). These factors make the OHC increase continuously, whose anomaly values are increased from 12.62×10^{22} J in May to 14.38×10^{22} J in September. Note that the highest PC1 (high OHC) in September may be primarily induced by the strong warm SCSTHT during July–August.

During October–December of a La Niña year, the wind field over the SCS has changed greatly. The strong northeasterly wind prevails over the northern SCS, while the southern SCS is primarily controlled by the southwesterly wind during October–November (Fig. 7d). In December, however, the strong northeasterly wind prevails over the waters north of 6°N, while weak northerly wind blows over the Sunda Shelf (not shown). Although the northeasterly wind

helps the upper surface water of the west Pacific and East China Sea enter the SCS, the northern SCS water still flows out of the SCS through the Luzon Strait and the Taiwan Strait. The stronger southerly or weaker northerly wind over the Sunda Shelf drives the warm water there into the SCS. Thus, the LSHT, TSHT, MSHT and SSHT are all a positive anomaly during October–December (Fig. 8a–d, black line). And the SCSTHT is also a positive anomaly but is weak (Fig. 8e, black line) primarily due to the weak LSHT and MSHT during this period. Meanwhile, the SCS still gets heat from the overlying atmosphere with a net surface heat flux anomaly range of 2.48–3.25×10^{10} W (Fig. 8f, black line). Therefore, the OHC still increase slowly with anomaly values 14.71–14.95×10^{22} J.

4.2. Mechanism for the OHC Regime Shift in 1998

The analysis of a t test with a 10-year running mean filter indicates that the OHC also experienced a regime shift in 1998. The mean OHC is $- 8.17 \times 10^{22}$ J during 1961–1998 and 23.34×10^{22} J during 1999–2012 with a difference of 31.51×10^{22} J. We next examine what processes are responsible for this.

Because there is an extremely strong El Niño event (warm event) and a strong La Niña event (cold event) during 1997–2000 (Cao et al. 2013), we can hypothesize the OHC regime shift may be associated with the warm and cold events. The Niño 4 index shows that the warm (cold) event started in April 1997 (July 1998) and ended in April 1998 (July 2000). In order to examine the mechanism for the OHC regime shift in 1998, we focus on the changes in the SCSTHT (including LSHT, TSHT, MSHT and SSHT) and the net surface heat flux during 1997–2000, respectively.

The SCSTHT is a negative anomaly during January 1997–February 1998 with a minimum of $- 12.07 \times 10^{13}$ W in May 1997, while it is a positive anomaly during March 1998–December 2000 with a maximum of 16.22×10^{13} W in September 1998 (not shown). The net surface heat flux is positive during July 1997–Mach 1998 with a maximum of 1.81×10^{13} W in February 1998, but it is all negative in other months with a minimum of

$- 3.52 \times 10^{13}$ W in October 1998 (not shown). Comparatively speaking, the SCSTHT has very consistent change with the OHC, but the net surface heat flux does not. A correlation analysis shows that during 1997–2000, the simultaneous relations between the OHC and the SCSTHT and the net surface heat flux reach 0.94 and $- 0.43$, respectively, suggesting that the OHC regime shift in 1998 is primarily induced by the SCSTHT. Since the simultaneous relations between the OHC and the LSHT, TSHT, MSHT and SSHE are 0.96, $- 0.17$, 0.69 and 0.41, respectively, the regime shift is mainly caused by the LSHT and MSHT. Specifically, the cold LSHT and MSHT lead to the sharp decrease of the OHC during the strong warm event, while the warm LSHT and MSHT lead to the sharp increase of the OHC during the strong cold event. As a result, the OHC experienced a regime shift from low to high in 1998.

In terms of interannual variability of the OHC in the SCS associated with ENSO, to sum up, the wind stress and the SCSTHT (LSHT, TSHT, MSHT and SSHT) are the main dynamic mechanisms, while the net surface heat flux is the main thermodynamic mechanism. The lowest PC1 (OHC) in June [0] may be primarily induced by the cold LSHT and the heat release of the SCS in May, while the highest PC1 (high OHC) in September [0] may primarily result from the strong warm SCSTHT during July–August. In addition, the OHC regime shift in 1998 is primarily caused by the strong cold LSHT and MSHT during the extremely strong El Niño in 1997 and the strong warm LSHT and MSHT during the strong La Niña in 1998.

5. Conclusions

Based on the monthly temperature and salinity data in the period of 1950–2012, the spatial and temporal variations of the OHC in the SCS and their relations to ENSO are analyzed using the EOF analysis method in this work. In addition, the mechanisms for OHC interannual variability and regime shift in 1998 are also examined using composite and correlation analysis methods based on SODA and NCEP data in the period of 1950–2012, respectively. The results obtained are as follows.

1. The OHC anomaly field in the SCS is mainly composed of an in-phase oscillation mode and a zonal anti-phase oscillation mode. The in-phase oscillation mode has a strong interannual variability with a period of 2–5 years and decadal oscillation with a period of 10 years, and it is well related to ENSO at a lead of 6 months. The anti-phase oscillation mode shows only a strong interannual variability with a period of 2–7 years and is well related to ENSO at a lag of 4 months.

2. The wind stress and the ocean thermal advection are the main dynamical mechanisms for the interannual variability in the OHC of the SCS associated with ENSO. The lowest PC1 (OHC) in June [0] may be primarily induced by the cold LSHT and the heat release of the SCS in May [0], while the highest PC1 (high OHC) in September [0] may primarily result from the strong warm SCSTHT during July–August [0].

3. The OHC of the SCS experienced a regime shift in 1998. The mean OHC during 1999–2012 is 31.51×10^{22} J higher than that during 1961–1998. The regime shift in 1998 is primarily caused by the strong cold LSHT and MSH during the extremely strong El Niño in 1997 and the strong warm LSHT and MSHT during the strong La Niña in 1998.

Publisher's Note   Springer Nature remains neutral with regard to jurisdictional claims in published maps and institutional affiliations.

References

Cai, R. S., Zhang, Q. L., & Qi, Q. H. (2009). Spatial and temporal oscillation and long-term variation in sea surface temperature field of the south china sea. *Journal of Oceanography in Taiwan Strait, 28*(4), 559–568. **(in Chinese with English abstract)**.

Cao, L., Sun, C. H., Ren, F. M., Yuan, Y., & Jiang, J. (2013). Study of a comprehensive monitoring index for two types of enso events. *Journal of Tropical Meteorology, 29*(1), 66–74. **(in Chinese with English abstract)**.

Carton, J. A., & Giese, B. S. (2008). A reanalysis of ocean climate using simple ocean data assimilation (soda). *Monthly Weather Review, 136*(8), 2999–3017.

Chen, X., Yan, Y. F., Cheng, X. H., et al. (2013). Performances of seven datasets in presenting the upper ocean heat content in the South China Sea. *Advances in Atmospheric Sciences, 30*(5), 1331–1342.

Chu, P. C., & Chang, C. P. (1997). South China Sea warm pool in boreal spring. *Advances in Atmospheric Sciences, 14*(2), 195–206.

Chu, P. C., Lu, S., & Chen, Y. (1997). Temporal and spatial variabilities of the south china sea surface temperature anomaly. *Journal of Geophysical Research Atmospheres, 1022*(C9), 20937–20956.

Fillenbaum, E. R., Lee, T. L., Johns, W. E., et al. (1997). Meridional heat transport variability at 26.5°N in the North Atlantic. *Journal of Physical Oceanography, 27,* 153–174.

Giese, B. S., & Ray, S. (2011). El niño variability in simple ocean data assimilation (SODA), 1871–2008. *Journal of Geophysical Research Oceans, 116*(C2), 1871–2008.

He, Y. H., & Guan, C. H. (1997). Interannual and interdecadal variability in heat cotent of the upper ocean of the South China Sea. *Journal of Tropic Oceanology, 16*(10), 23–29. **(in Chinese with English abstract)**.

Ishii, M., Kimoto, M., Sakamoto, K., & Iwasaki, S. I. (2006). Steric sea level changes estimated from historical ocean subsurface temperature and salinity analyses. *Journal of Oceanography, 62*(2), 155–170.

Ishii, M., Kimotom, M., & Kachim, M. (2003). Historical ocean subsurface temperature analysis with error estimates. *Monthly Weather Review, 131*(1), 51–73.

Jin, Z. H., & Luo, S. H. (1986). On the relationship between rainfall anomaly in middle and lower Yangtze valley during the Mei-yu season and the anomaly of sea-surface temperature in South

China Sea. *Acta Meteorologica Sinica, 44,* 368–372. **(in Chinese with English abstract)**.

Johns, W. E., Baringer, M. O., Beal, L. M., et al. (2011). Continuous, array-based estimates of Atlantic Ocean heat transport at 26.5°N. *Journal of Climate, 24*(10), 2429–2449.

Kalnay, E., Kanamitsu, M., Kistler, R., Collins, W., Deaven, D., Gandin, L., et al. (1996). The ncep/ncar 40-year reanalysis project. *Bulletin of the American Meteorological Society, 77*(3), 437–472.

Klein, S. A., Soden, B. J., & Lau, N. C. (1999). Remote sea surface temperature variations during enso: evidence for a tropical atmospheric bridge. *Journal of Climate, 12*(12), 917–932.

Lai, Z. J., Peng, S. Q., Li, Y. N., & Liu, Q. Y. (2011). Relationship between summer monsoon outbreak and upper-ocean heat content anomalies over the South China Sea. *Journal of Tropical Oceanopraphy, 30*(6), 47–56. **(in Chinese with English abstract)**.

Niu, Z. W. (1994). The long-term oscillation of the SST in the South China Sea and its relationship to El Niño. *Acta Oceanologica Sinica, 16*(2), 43–49. **(in Chinese with English abstract)**.

Ose, T., Song, Y., & Kitoh, A. (1997). Sea surface temperature in the South China Sea: an index for the Asian monsoon and ENSO system. *J. Metor. Soc. Japan, 75,* 1091–1107.

Peter, C. C., Lu, S. H., & Chen, Y. C. (1997). Temporal and spatial variabilities of the South China Sea surface temperature anomaly. *Journal of Geophysical Research, 102*(C9), 20937–20955.

Qi, Q. H., & Cai, R. S. (2014). The relation between the spatial-temporal evolution of SST in the South China Sea and the earlier or later onset of the South China Sea summer monsoon. *Acta Oceanologica Sinica, 36*(3), 94–103. **(in Chinese with English abstract)**.

Qu, T. D., Kim, Y. Y., Yaremchuk, M., Tozuka, T., Ishida, A., & Yamagata, T. (2004). Can Luzon strait transport play a role in conveying the impact of ENSO to the South China Sea? *Journal of Climate, 17*(18), 3644–3657.

Song, W., Lan, J., Liu, Q. Y., & Wang, D. X. (2014). Decadal variability of heat content in the South China Sea inferred from observation data and an ocean data assimilation product. *Ocean Science, 10*(4), 135–139.

Tong, J. Q., Wang, J., & Qi, Y. Q. (2006). Interannual variability of the heat storage anomaly in the South China Sea estimated from merged altimetric data. *Chinese Journal of Geophysics., 49*(6), 1651–1656. **(in Chinese with English abstract)**.

Wang, B., Ho, L., Zhang, Y. S., & Lu, M. M. (2004). Definition of South China Sea monsoon onset and commencement the East Asia summer monsoon. *Journal of Climate, 17*(4), 699–710.

Wang, Q., Liu, Q. Y., Hu, R. J., & Xie, Q. (2002). A possible role of the South China Sea in ENSO cycle. *Acta Oceanologica Sinica, 21*(2), 217–226.

Wang, C. Z., Wang, W. Q., Wang, D. X., & Wang, Q. (2006). Interannual variability of the South China Sea associated with El Niño. *Journal of Geophysical Research, 111,* (C03023). https://doi.org/10.1029/2005JC003333.

Wang, B., Wu, R., & Fu, X. (2000). Pacific-east asian teleconnection: how does enso affect east asian climate. *Journal of Climate, 13*(9), 1517–1536.

Wu, X. F., Xu, J. P., Zhang, Q. L., & Sun, Z. H. (2011). A preliminary study on upper ocean heat content of tropical western Pacific. *Marine Forecasts, 28*(4), 76–86. **(in Chinese with English abstract)**.

Xie, S. P., Xie, Q., Wang, D. X., & Liu, W. T. (2003). Summer upwelling in the South China Sea and its role in regional climate variations. *Journal of Geophysical Research, 108*(c8), 343–367.

Yan, Y. F., Qi, Y. Q., & Zhou, W. (2010). Interannual heat content variability in the South China Sea and its response to ENSO. *Dynamics of Atmospheres and Oceans, 50*(3), 400–414.

Zhang, Q., Liu, P., & Wu, G. X. (2003). The relationship between the flood and drought over the lower reach of the Yangtze River Valley and the SST over the Indian Ocean and the South China Sea. *Chinese Journal of Atmospheric Sciences, 27*(6), 992–1006. **(in Chinese with English abstract)**.

Zhao, Y. P., & Chen, Y. L. (2000). The seasonal and inter-annual variability of the South China Sea warm pool and its relation to the South China Sea monsoon onset. *Journal of Tropical Meteorology, 16*(3), 202–211. **(in Chinese with English abstract)**.

Zhou Y. X. (2002). Statistical analysis of ocean thermocline in the South China Sea. In graduate thesis of Qingdao Ocean University, 1–59 (in Chinese with English abstract).

Zhou, L. T., Tam, C. Y., Zhou, W., & Chan, J. C. L. (2010). Influence of South China Sea SST and the ENSO on winter rainfall over South China. *Advaces in Atmospheric Sciences, 27*(4), 832–844.